Electronic Supplementary Material (ESI) for Journal of Materials Chemistry B.
This journal is © The Royal Society of Chemistry 2021

Electronic Supplementary Information (ESI)
For

Structural Diversity of Nanoscale Zirconium Porphyrin MOFs and Their Photoactivities and Biological Performances

Junli Zhou,[a,b] *Yite Li,*[a,b] *Lei Wang,**[a] *Zhigang Xie,**[a,b]

[a] State Key Laboratory of Polymer Physics and Chemistry, Changchun Institute of Applied Chemistry, Chinese Academy of Sciences, Changchun 130022, People's Republic of China

[b] University of Science and Technology of China, Hefei 230026, People's Republic of China

Email: leiwang@ciac.ac.cn; xiez@ciac.ac.cn

Table of Contents

Section S1. Materials and methods

Chemicals. All chemical materials (2, 2-dichloroacetic acid, and Zirconyl chloride octahydrate, Meso-Tetra (4-carboxyphenyl) porphyrin (TCPP), Acetic acid, and benzoic acid) and N, N-dimethylformamide (DMF) used were purchased commercially without further purification. Live-Dead Cell Staining Kit was purchased from Nanjing KeyGen Biotech Co., Ltd. MTT (3-[4, 5-dimethylthiazol-2-yl]-2, 5-diphenyltetrazoliumbromide) and Annexin V-FITC Apoptosis Detection Kit was purchased from Beyotime Biotechnology Co., Ltd.

Analytical techniques. TEM images of as-synthesized TCPP-MOFs nanoparticles were captured with a JEOL JEM-1011 electron microscope operated at an acceleration voltage of 100 kV. Powder X-ray diffraction (PXRD) patterns were recorded on a modified Xeuss SAXS/WAXS system of Xenocs France equipped with a semiconductor detector (Pilatus 100 K, DECTRIS, Swiss) attached to a multilayer focused Cu Kα X-ray source (GeniX3D Cu ULD, Xenocs SA, France), generated at 50 kV and 0.6 mA. Each pattern was collected in 60 s, and the background was subtracted. Size, size distribution and zeta-potential of the nanoparticles were determined by Malvern Zeta-sizer Nano (Section S3). FT-IR was collected with VERTEX 70 Fourier Transform Infrared Spectrometer (Section S3). The UV−vis spectrum was collected with a Shimadzu UV-2450 spectrometer (Section S3). Fluorescence intensity tests were performed using Perkin Elmer LS-55 fluorospectrophotometer. Fluorescence lifetime and steady state spectroscopy were performed using time-correlated single-photon counting (TCSPC) method and collected on an Edinburgh FLS980, with an Edinburgh EPL-400 picosecond pulsed diode laser as the excitation source. Fluorescence and confocal microscopy (CLSM) images were taken using Zeiss LSM 700 (Zurich, Switzerland). Flow cytometry

analyses were recorded by a flow sight cytometry imaging system (Amnis). Inductively coupled plasma mass spectrometry (ICP-MS) was carried out on an Agilent 7700x series ICP-MS instrument. Safety evaluation was carried out by the automatic biochemical analyzer (Mindray, BS-220). Blood routine examinations were carried out by an automatic blood cell analyzer (ABX MICROS 60). Plasma coagulation study was carried out by an automatic coagulation analyzer (ACL TOP500). Nitrogen adsorption-desorption experiments are characterised by Micromeritics (ASAP).

Section S2. Size control of TCPP-MOFs isomers

MOF-525. Zirconyl chloride octahydrate (5.2 mg), TCPP (9.8 mg), and 0.25 mL of acetic acid in 3 mL of DMF were ultrasonically dissolved in a Pyrex vial. The mixture was heated in 90 °C oven for 18 h. After cooling down to room temperature cubic dark purple solid were harvested by filtration. FT-IR: 3398, 1700, 1605, 1540, 1403, 1179, 1103, 1019, 982, 963, 868, 799, 772, 720, 650, 474 cm^{-1}

PCN-222. Zirconyl chloride octahydrate (37.5 mg), TCPP (6.5 mg), and 0.25 mL of 2, 2-dichloroacetic acid in 16 mL of DMF were ultrasonically dissolved in a Pyrex vial. The mixture was heated in 130 °C oven for 18 h. After cooling down to room temperature cubic dark purple solid were harvested by filtration. FT-IR: 3403, 1701, 1606, 1544, 1408, 1178, 1101, 1042, 1019, 985, 963, 868, 821, 797, 772, 719, 652, 473 cm^{-1}

PCN-223. In a 25 mL round-bottom flask, Zirconyl chloride octahydrate (9.8 mg), TCPP (5.2 mg), and 0.25 mL of acetic acid were dissolved in DMF (3 mL). The mixture was heated in 90 °C oven for 18 h. After cooling down to room temperature cubic dark purple solid were harvested by filtration. FT-IR: 3395, 1701, 1604, 1548, 1409, 1178, 1102, 1019, 983, 963, 868, 798, 772, 721, 648, 473 cm^{-1}

PCN-224. In a 250 mL round-bottom flask, Zirconyl chloride octahydrate (299.7 mg), TCPP (102.8 mg), and 2.8 g of benzoic acid were dissolved in DMF (100 mL). The mixture was heated in 90 °C oven for 3 h. After cooling down to room temperature cubic dark purple solid were harvested by filtration. FT-IR: 3392, 1700, 1602, 1545, 1416, 1177, 1101, 1042, 1019, 981, 963, 868, 798, 771, 720, 652, 458 cm^{-1}

Section S3. Characterization

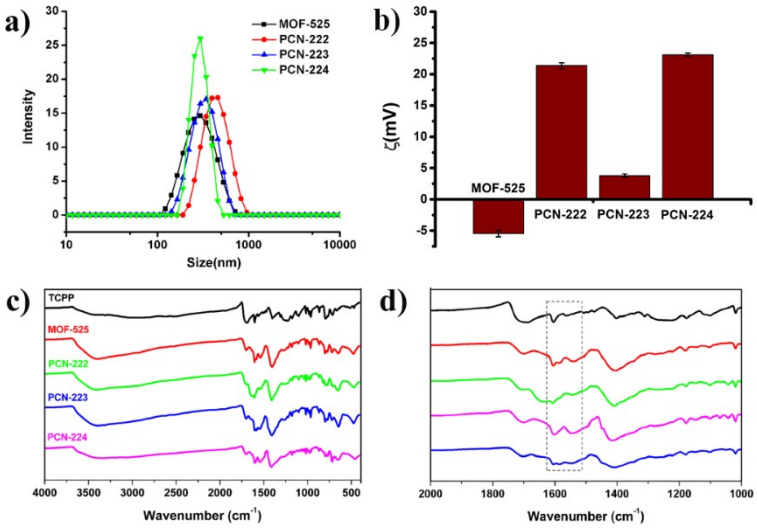

Figure S1. (a) Dynamic light scattering (DLS) profile of as-synthesized TCPP-MOF isomers dispersed in water. (b) zeta potentials of as-synthesized TCPP-MOF isomers dispersed in water. (c-d) Overlay of FT-IR spectra of as-synthesized TCPP-MOF isomers and theirs corresponding detail absorption from 2000 to 1000 cm^{-1}, respectively.

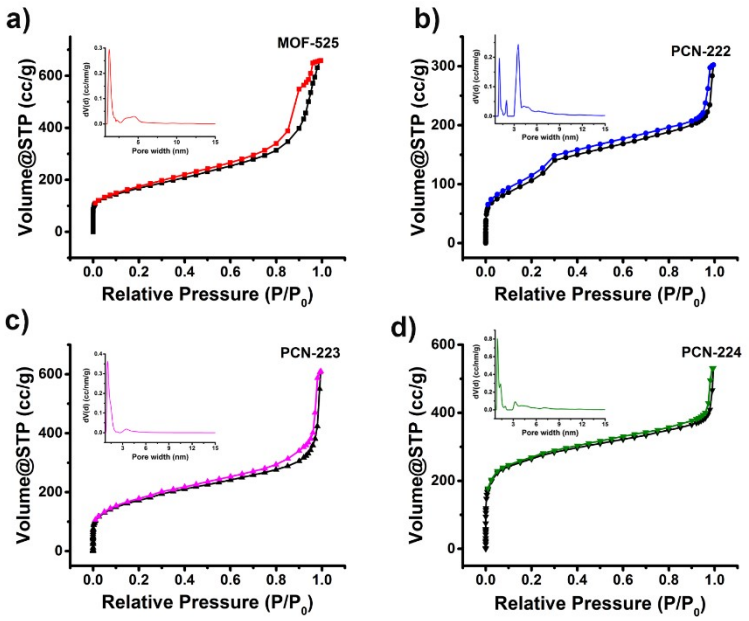

Figure S2. Nitrogen adsorption-desorption curves of TCPP-MOFs at 77 K. (a) MOF-525. (b) PCN-222. (c) PCN-223. (d) PCN-224. The as-synthesized TCPP-MOFs were exchanged for solvent with methanol three times in 2 d, and then dried in vacuum at 40 ^{o}C for 24 h.

Table S1. Pore structure parmeters of TCPP-MOFs samples.

Materials	MOF-525	PCN-222	PCN-223	PCN-224
Multipoint BET(m^2/g)	593	396	612	973
Pore width (nm)	1.24	1.05, 3.55	1.10	0.93

Table S2. The photophysical parameters of TCPP-MOF isomers

Sample	Max absorption (nm)	Emission (nm)	Bi-exponential fitting		<τ>[c] (ns)	Quantum yield
			$\tau_1(\alpha_1)$[b] (ns)[a]	$\tau_2(\alpha_2)$[b] (ns)[a]		
TCPP	419	655, 718	14.59 (50%)	14.59 (50%)	14.59	0.109
MOF-525	420	655, 718	1.32 (99.9%)	2.42 (0.06%)	1.32	0.035
PCN-222	424	656, 720	1.09 (99.9%)	2.28 (0.002%)	1.09	0.035
PCN-223	418.5	656, 720	2.32 (98.6%)	4.38 (8.44%)	2.36	0.076
PCN-224	422	656, 716	2.02 (0.004%)	1.06 (99.9%)	1.06	0.067

[a] Lifetimes excitation at 410 nm. [b] Relative amplitude. [c] Average lifetime.

Section S4. *In vitro* singlet-oxygen generation

Three capture agents of 1,3-diphenylisobenzofuran (DPBF), anthracene (An), and ICG with different molecular size have been selected and monitored at each featured UV absorption of those above agents, respectively.[S1-2] Taking DPBF as an example, an amount of 3 mL of DMF containing 50 μL of DPBF (1 mg mL^{-1}) and TCPP-MOFs isomers (4 μM TCPP) in a quartz cuvette was fully mixed for six hours in the darkness, and then irradiation by 635 nm laser lamp (0.47 W cm^{-2}) at room temperature. The absorption intensity of DPBF at 410 nm in the mixture was recorded at five-seconds intervals. The rate of singlet oxygen generation was determined from the reduced absorbance intensity over time. For the control experiments, DPBF alone and molecular TCPP at the same concentration were measured at the same condition. Similarly, An (15 μg ml^{-1}) and ICG (20 μg ml^{-1}) were used and monitored at 359 and 791 nm at the same experimental conditions, respectively.

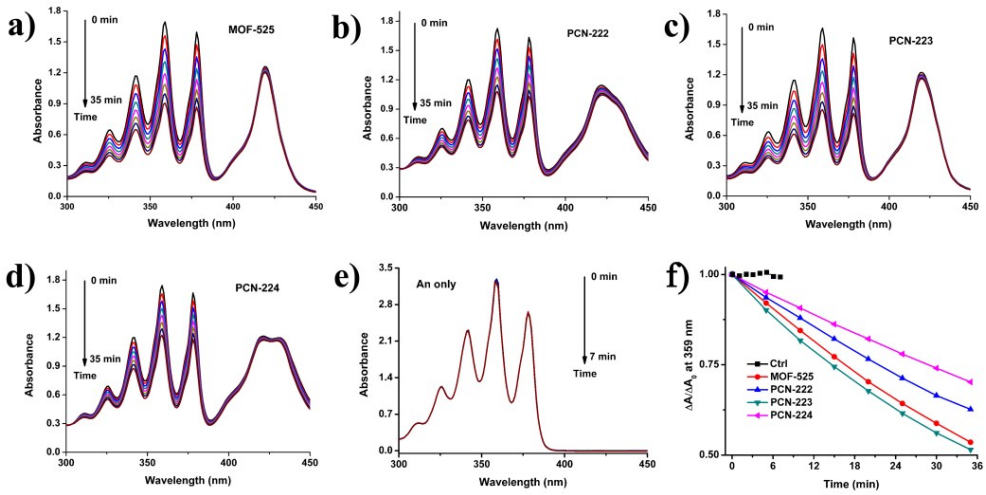

Figure S3. Time-dependent UV-Vis absorption spectra of An blending with (a) MOF-525, (b) PCN-222, (c) PCN-223, (d) PCN-224, and (e) An only dispersed in DMF upon laser irradiation, respectively. (f) Comparison of the decay rate of An after treated with TCPP-MOF experimental groups and An control group.

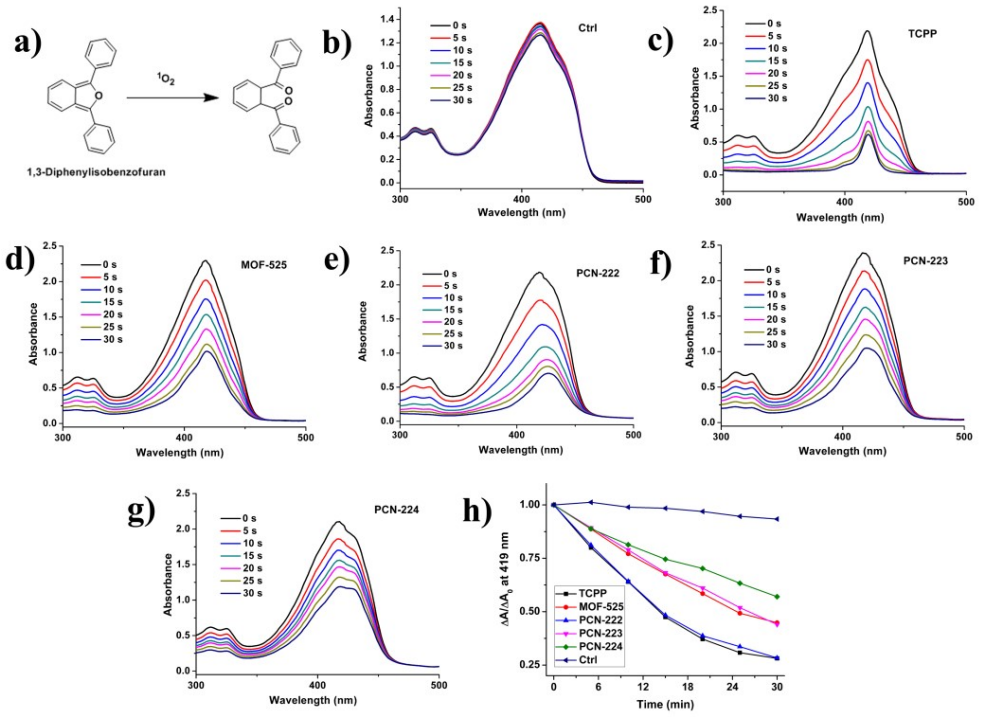

Figure S4. (a) Reaction mechanism of DPBF with $^1O_2$. Time-dependent UV-Vis absorption spectra of DPBF blending with (b) blank control, (c) TCPP control, (d) MOF-525, (e) PCN-222, (f) PCN-223, and (g) PCN-224 dispersed in DMF upon laser irradiation, respectively. (h) Comparison of the decay rate of DPBF after treated with TCPP-MOF experimental groups and control groups.

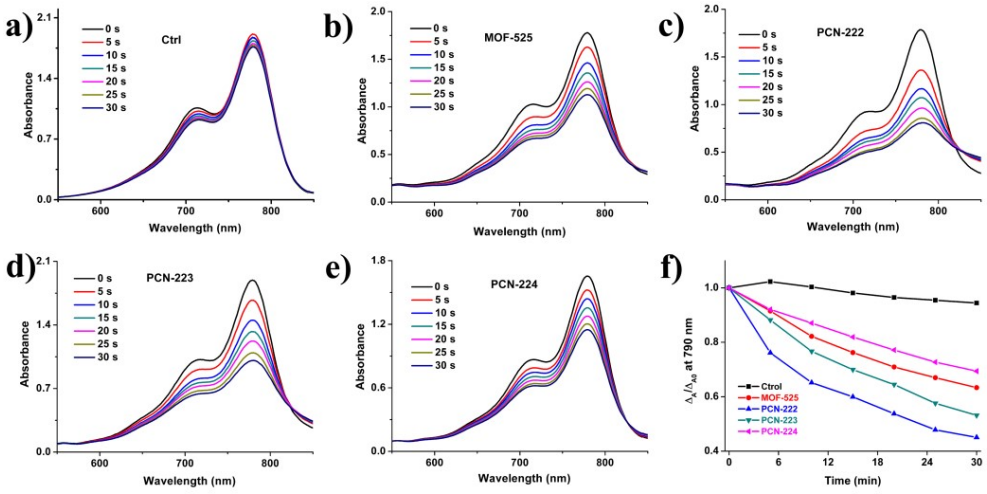

Figure S5. Time-dependent UV-Vis absorption spectra of ICG blending with (a) blank control, (b) MOF-525, (c) PCN-222, (d) PCN-223, and (e) PCN-224 dispersed in water upon laser irradiation, respectively. (f) Comparison of the decay rate of ICG after treated with TCPP-MOF experimental groups and control groups.

Section S5. Photothermal measurements

TCPP-MOF isomers samples with the same TCPP concentration of 40 μM dispersed in water were irradiated with a 635 nm laser at intensity of 0.47 W cm^{-2} for 300 s. Deionized water was measured as a control at the same condition. More precisely, the temperature changes of the solution were monitored by a thermocouple probe. The thermocouple probe and the laser path keep a parallel direction. Secure digital (SD) card was used to record the data every 10 s.

Section S6. Structure diagram of the dihedral angle ($\theta_{\text{di-tcpp}}$) between the porphyrin ring and phenyl group

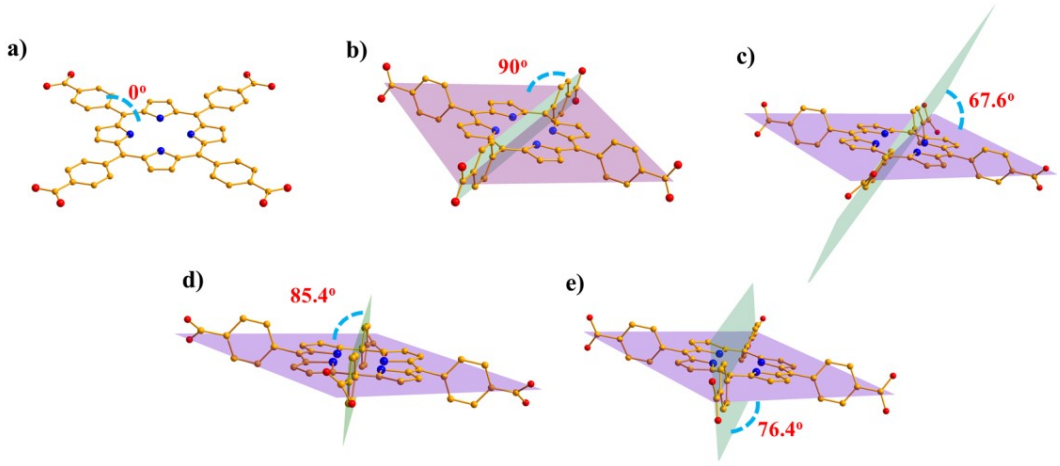

Figure S6. Structural diagram of the dihedral angle ($\theta_{\text{di-tcpp}}$) between the porphyrin ring and phenyl group coming from each corresponding single crystal structure modes of TCPP-MOF structures [S3-6].

Section S7. Computational details

Two adjacent TCPP dimers from the four tested structures (MOF-525, PCN-222, PCN-223, and PCN-224) were selected and further optimizated according to previous work.[S7-8] The theory calculations were done by using the B97X-D/def2-SVP. DFT optimized structures of closely positioned TCPP dimers from the four tested Zr-TCPP MOFs are listed in the Figure S6. And the selected TD-DFT computed transitions for monomeric TCPP and each TCPP-dimer and its frontier orbitals are given in Table S2 and Figure S7-10, respectively.

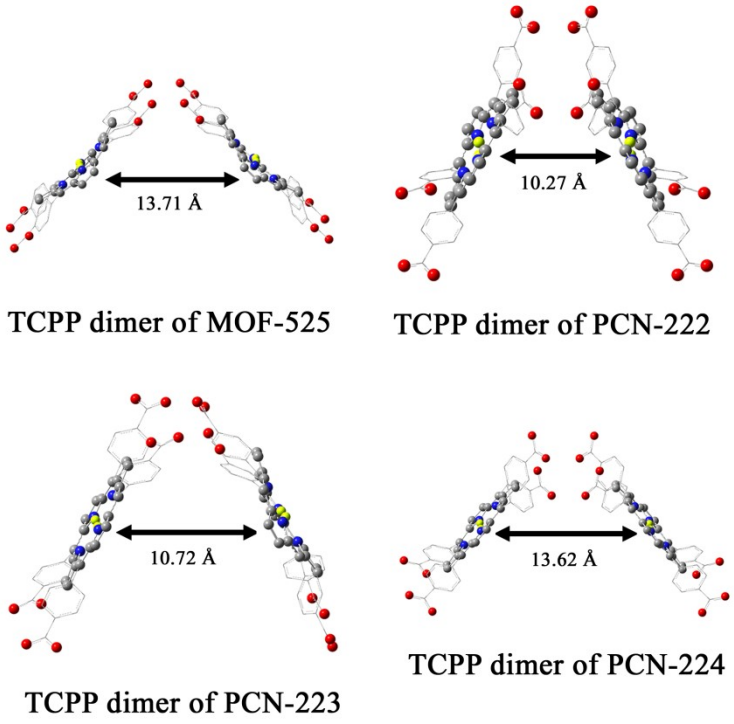

Figure S7. DFT optimized structures of closely positioned TCPP dimers from the four tested Zr-TCPP MOFs. (a) MOF-525, (b) PCN-222, (c) PCN-223, and (d) PCN-224, respectively. H atoms connected to C and O are omitted for clarity.

Table S3. Selected TD-DFT computed transitions for monomeric TCPP and TCPP-dimer of MOF-525, PCN-222, PCN-223, and PCN-224. (H and L are clarity to HOMO and LUMO, respectively.

Species	Excited state	Transition energy (eV)	Wavelength (nm)	Oscillator Strength	MOs involved in the transitions
TCPP	1	2.0570	602.74	0.0081	H-1→L(41.2%); H→L+1(58.7%)
	2	2.2755	544.86	0.0239	H-1→L+1(42.1%); H→L(57.3%)
	3	3.3772	367.13	1.4186	H-3→L+1(8.7%); H1→L(55.4%); H→L+1(35.4%); H←L+1(2.5%)
	4	3.4713	357.17	1.8433	H-1→L+1(57.7%); H→L(43.0%); H-1←L+1(2.0%); H←L(2.9%)
MOF-525	1	1.9145	647.61	0.0000	H-3→L+1(18.4%);H-2→L(18.4%); H-1→L+3(30.6%);H→L+2(30.8%)
	2	1.9180	646.44	0.0587	H-3→L(19.0%);H-2→L+1(18.9%); H-1→L+2(30.1%);H→L+3(30.2%)
	3	2.1100	587.61	0.1438	H-3→L+3(16.5%);H-2→L+2(16.5%); H-1→L+1(32.4%);H→L(32.8%)
	4	2.1188	585.16	0.0987	H-3→L+2(17.4%);H-2→L+3(17.4%); H-1→L(31.6%);H→L+1(31.7%)
	5	3.1414	394.68	0.0000	H-8→L+3(2.5%);H-7→L+2(2.4%); H-3→L+1(29.4%);H-2→L(29.7%); H-1→L+3(16.6%);H←L+2(17.3%)
	6	3.2100	386.24	2.7337	H-8→L+2(3.8%);H-7→L+3(3.7%); H-3→L(28.7%);H-2→L+1(28.5%); H-1→L+2(16.9%);H←L+3(16.8%)
	7	3.2360	383.14	2.0427	H-3→L+3(32.2%);H-2→L+2(32.4%); H-1→L+1(16.8%);H→L(17.7%)
	8	3.3122	374.32	1.6584	H-3→L+2(31.6%);H-2→L+3(31.4%); H-1→L(18.4%);H→L+1(18.3%)
PCN-222	1	2.0328	609.92	0.0000	H-3→L+1(19.2%);H-2→L(19.2%); H-1→L+3(30.4%);H→L+2(30.6%)
	2	2.0354	609.15	0.0297	H-3→L(19.7%);H-2→L+1(19.7%); H-1→L+2(30.0%);H→L+3(30.0%)
	3	2.2444	552.42	0.0238	H-3→L+3(19.8%);H-2→L+2(19.9%); H-1→L+1(29.6%);H→L(29.8%)
	4	2.2488	551.33	0.0531	H-3→L+2(20.4%);H-2→L+3(20.4%); H-1→L(29.2%);H→L+1(29.2%)
	5	3.3018	375.51	0.0000	H-7→L+3(2.6%);H-6→L+2(2.5%); H-3→L+1(29.4%);H-2→L(29.8%); H-1→L+3(17.1%);H←L+2(17.6%)
	6	3.3553	369.51	1.0419	H-3→L+3(29.7%);H-2→L+2(30.1%); H-1→L+1(20.0%);H→L(20.6%)
	7	3.3853	366.24	2.5458	H-7→L+2(4.2%);H-6→L+3(4.0%); H-3→L(28.4%);H-2→L+1(28.2%); H-1→L+2(17.1%);H←L+3(16.9%)
	8	3.4849	355.77	2.6662	H-3→L+2(29.5%);H-2→L+3(29.3%); H-1→L(21.1%);H→L+1(20.8%)
PCN-223	1	1.9889	623.38	0.0003	H-3→L(34.6%);H-2→L+3(5.2%); H-1→L+1(47.7%);H→L+2(9.5%)
	2	1.9932	622.02	0.0348	H-3→L(7.4%);H-2→L+2(3.8%); H-2→L+3(26.3%);H1→L+1(9.4%); H→L+2(45.8%);H→L+3(6.2%)
	3	2.2044	562.44	0.0447	H-3→L+1(28.2%);H-2→L+2(10.0%); H1→L(41.7%);H→L+2(2.2%); H→L+3(15.4%)
	4	2.2107	560.83	0.0592	H-3→L+1(12.3%);H-2→L+2(25.2%); H-2→L+3(3.3%);H1→L(16.6%);

					H→L+2(5.3%);H→L+3(36.2%)
	5	3.2345	383.32	0.0014	H-10→L+1(3.5%);H-3→L(27.8%); H-2→L+2(4.5%);H-2→L+3(26.0%); H1→L+1(18.4%);H→L+2(13.3%); H→L+3(2.6%)
	6	3.3104	374.53	1.1130	H-3→L+1(23.7%);H-2→L+2(32.2%); H-2→L+3(3.9%);H1→L(16.1%); H→L+2(2.5%);H→L+3(21.3%)
	7	3.3213	373.31	2.4487	H-10→L+1(5.5%);H-7→L+2(2.3%); H-3→L(25.7%);H-2→L+2(2.8%); H-2→L+3(27.4%); H-1→L+1(17.2%);H→L+2(14.7%)
	8	3.4170	362.84	2.7583	H-3→L+1(34.8%);H-2→L+2(19.8%); H-2→L+3(3.7%);H1→L(25.3%); H→L+2(2.5%);H→L+3(14.3%)
PCN-224	1	2.0615	601.41	0.0000	H-3→L+1(20.2%);H-2→L(20.2%); H-1→L+3(29.6%);H→L+2(29.6%)
	2	2.0625	601.14	0.0152	H-3→L(20.5%);H-2→L+1(20.5%); H-1→L+2(29.4%);H→L+3(29.4%)
	3	2.2762	544.71	0.0300	H-3→L+3(20.6%);H-2→L+2(20.6%); H-1→L+1(29.1%);H→L(29.1%)
	4	2.2783	544.2	0.0242	H-3→L+2(20.9%);H-2→L+3(20.9%); H-1→L(28.7%);H→L+1(28.8%)
	5	3.3500	370.1	0.0000	H-7→L+3(3.4%);H-6→L+2(3.4%); H-3→L+1(28.3%);H-2→L(28.4%); H-1→L+3(17.8%);H→L+2(17.9%)
	6	3.4044	364.19	2.6353	H-7→L+2(4.5%);H-6→L+3(4.5%); H-3→L(27.7%);H-2→L+1(27.6%); H-1→L+2(17.6%);H→L+3(17.6%)
	7	3.4264	361.85	1.7913	H-3→L+3(29.2%);H-2→L+2(29.2%); H-1→L+1(20.8%);H→L(21.0%)
	8	3.5046	353.77	1.9911	H-3→L+2(29.0%);H-2→L+3(28.9%); H-1→L(21.4%);H→L+1(21.3%)

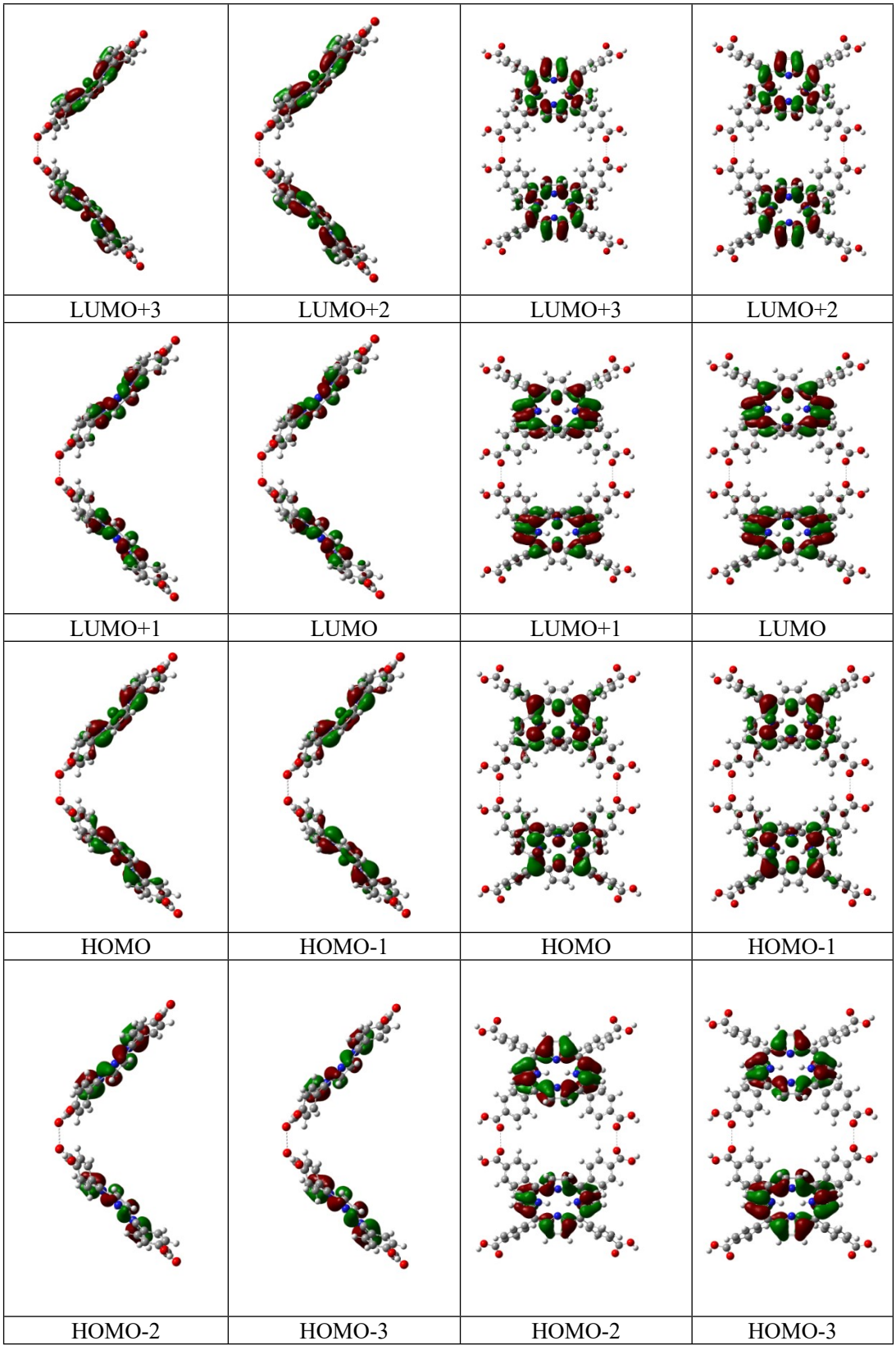

Figure S8. Frontier orbitals of MOF-525 (left) side and (right) front view highlighting shared electronic density in the FMOs due to strong interaction.

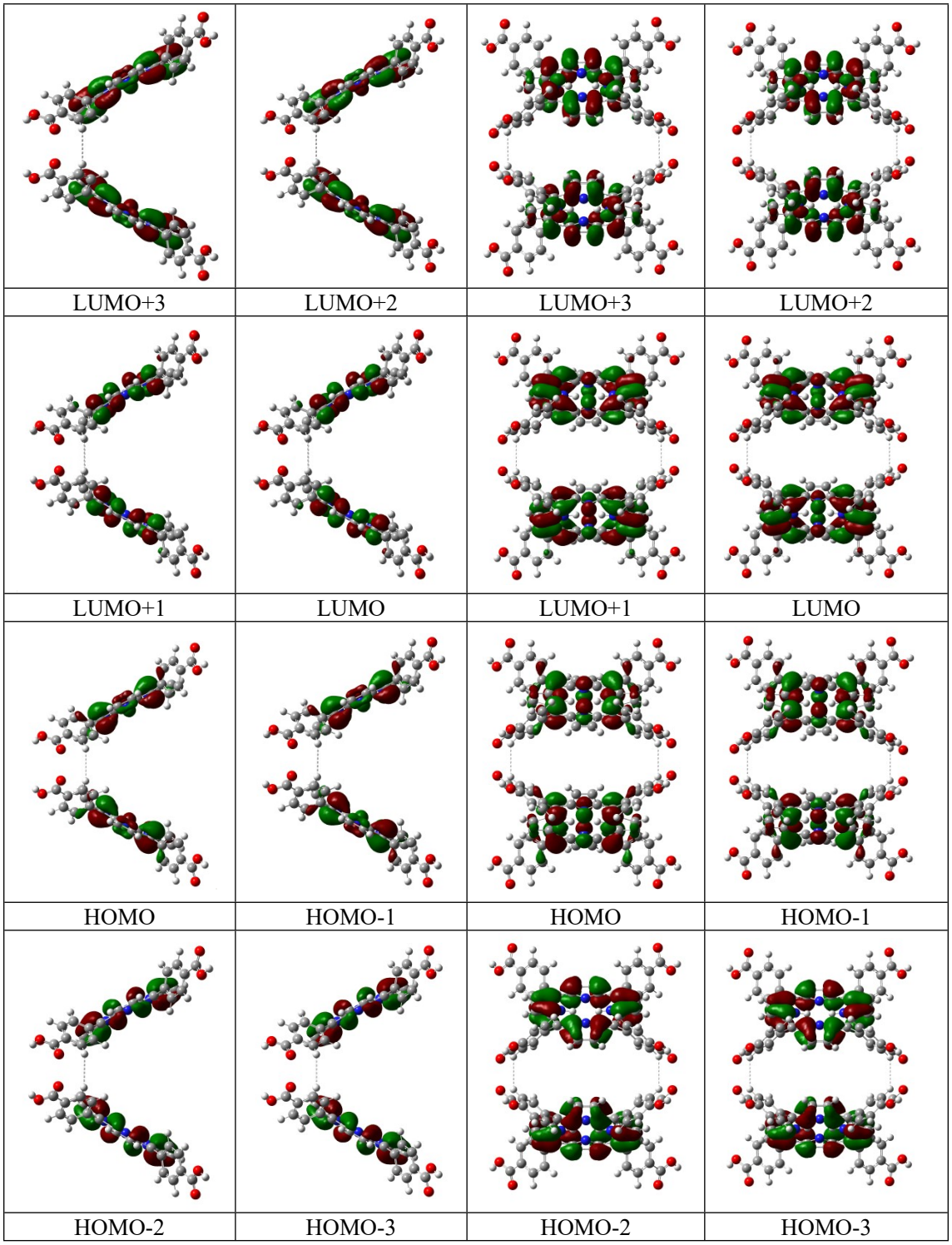

Figure S9. Frontier orbitals of PCN-222 (left) side and (right) front view highlighting shared electronic density in the FMOs due to strong interaction.

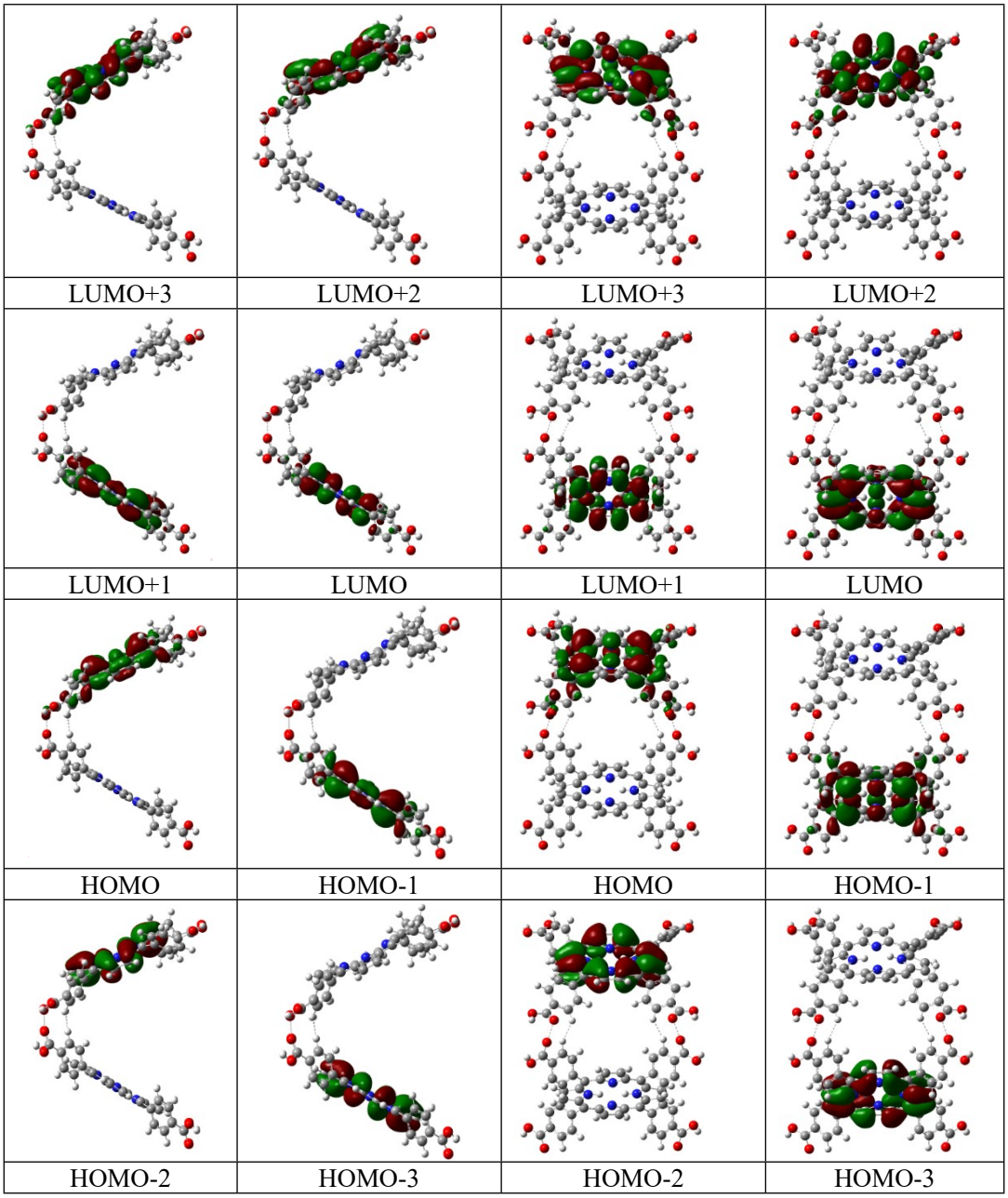

Figure S10. Frontier orbitals of PCN-223 (left) side and (right) front view highlighting shared electronic density in the FMOs due to strong interaction.

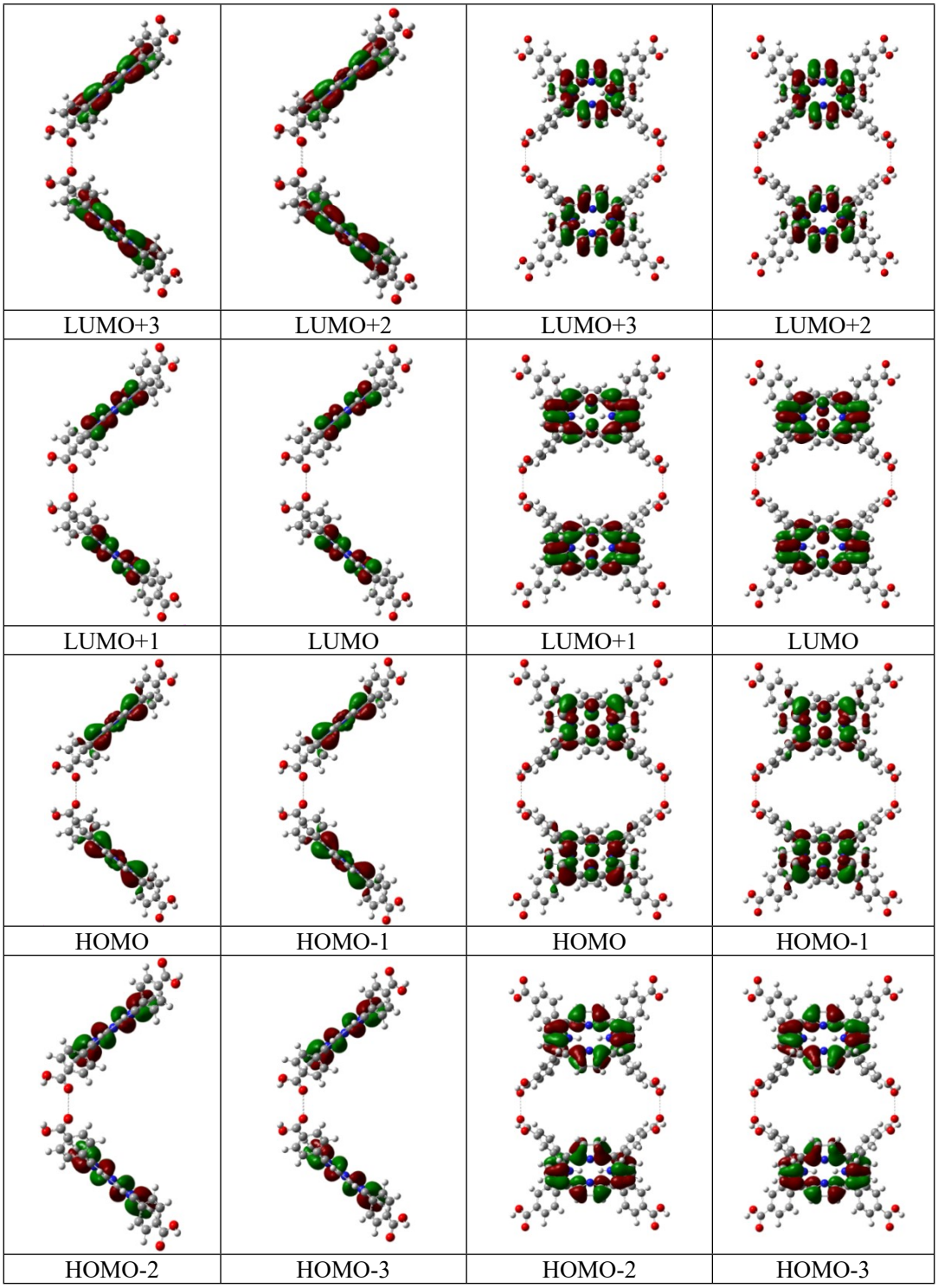

Figure S11. Frontier orbitals of PCN-224 (left) side and (right) front view highlighting shared electronic density in the FMOs due to strong interaction.

Section S8. *In vitro* experiments

Cell culture

The human cervical carcinoma HeLa cells and human mammary cancer MCF-7 cells were cultured at 37 °C in a humidified atmosphere containing 5% (v/v) CO_2 in Dulbecco's modified Eagle medium (DMEM, GIBCO) supplemented with 10% fetal bovine serum (GIBCO) and 100 U mL^{-1} penicillin and 100 mg mL^{-1} streptomycin.

Cellular uptake

The HeLa cells and MCF-7 cells were cultured with TCPP-MOF isomers samples (40 μM TCPP) for different time (0.5, 1, and 2 h), respectively. Subsequently, the supernatant was removed and the cells were washed gently three times with PBS (pH 7.4), fixed with 4% paraformaldehyde for 10 min at ambient temperature and washed thrice with cold PBS. Hoechst 33258 was employed to counterstain the cell nuclei. For CLSM test, Hoechst 33258 was excited by 405 laser while TCPP-MOF samples was excited by 488 nm laser. The uptake amount of each TCPP-MOF samples were measured by UV−vis spectrum. Cells were washed, harvested and collected. The cells were digested with 200 μL of concentrated phosphoric acid. Free TCPP ligand was extracted with 600 μL of DMSO and the concentrations were determined by UV-Vis absorption at 420 nm.

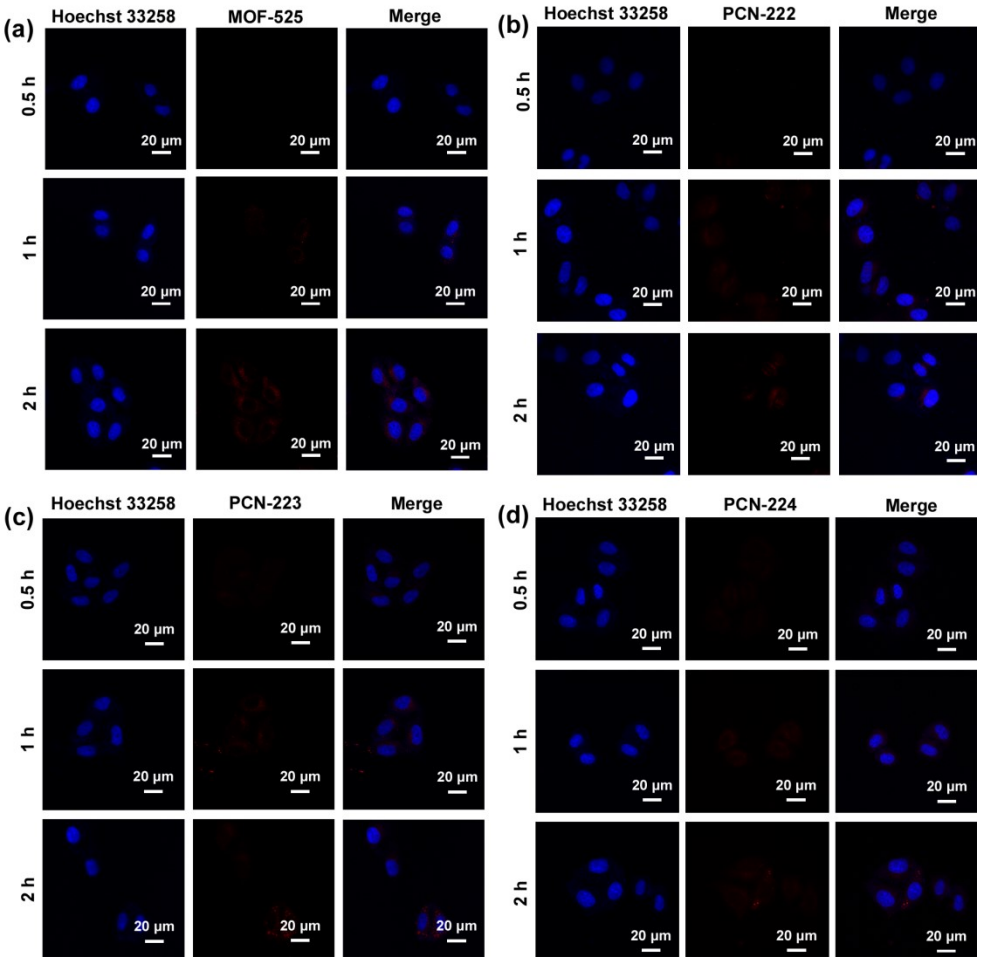

Figure S12. *In vitro* confocal laser scanning microscopy (CLSM) images of HeLa cells treated with TCPP-MOFs isomers with the same TCPP concentration of 40 μM for 0.5, 1, and 2 h at 37 °C.

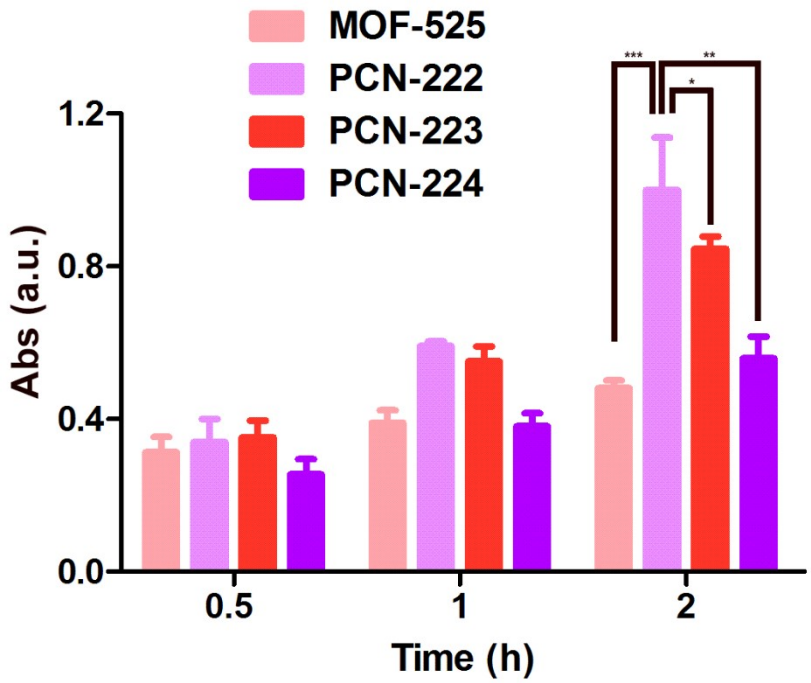

Figure S13. Cellular uptake of TCPP-MOF samples in MCF-7 cell line at different time points. Data are based on UV-Vis absorption of TCPP internalized into MCF-7 cells. TCPP concentration of 40 μM for 2 h at 37 °C. Asterisks indicate significantly differences (*P < 0.05, **P < 0.01).

Internalization mechanism of MOFs

To determine the endocytosis pathways, HeLa cells and MCF-7 cells were incubated with different inhibitors for 1 h. That is, sucrose (450 mM, inhibitor of clathrin-mediated endocytosis), amiloride (0.32 mM, inhibitor of Na^+/H^+ pump related macropinocytosis) and genistein (0.10 mM, inhibitor of lipid raft-caveolae endocytosis) were used.[S9-10] After incubation with each TCPP-MOF samples (40 μM) for additional 2 h, cells were washed, harvested and collected. The cells were digested with 200 μL concentrated phosphoric acid. Free TCPP ligand was extracted with 600 μL DMSO and the concentrations were determined by UV-Vis absorption at 420 nm.

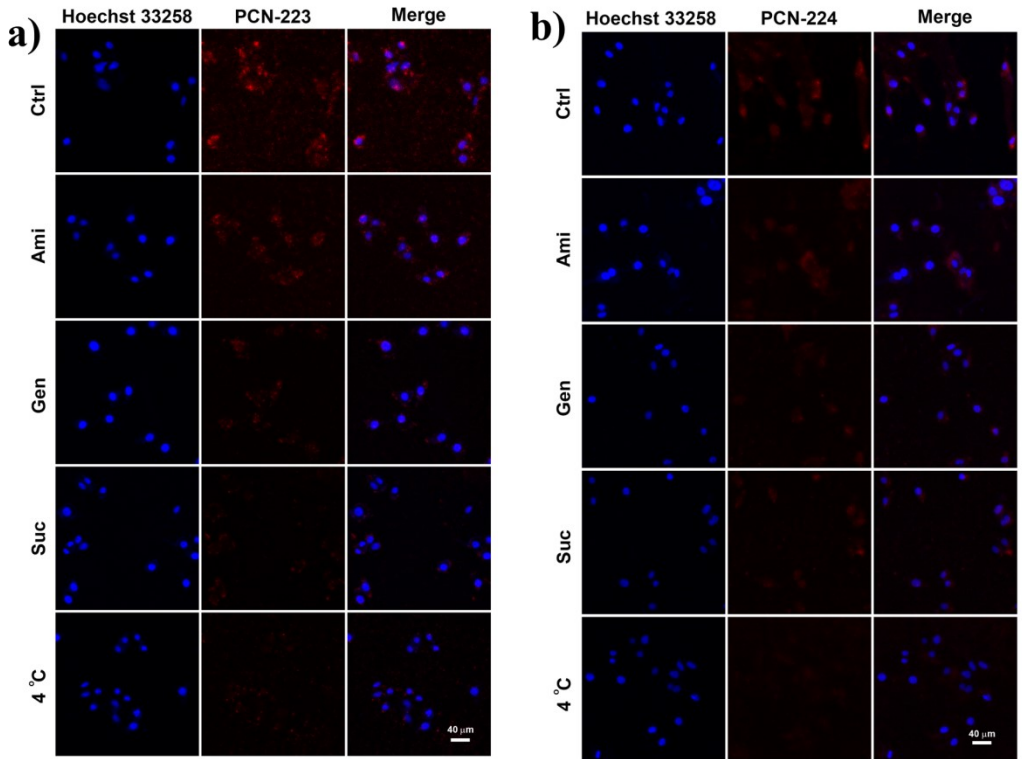

Figure S14. CLSM images of PCN-223 and PCN-224 incubated with HeLa cells by adding different inhibitors at the same TCPP concentration of 40 μM for 2 h at 37 °C. Sucrose (SUC) for clathrin-mediated endocytosis, genistein (GEN) for caveolin mediated endocytosi, amiloride (AMI) for macropinocytosis, and 4 °C for energy-mediated endocytosis, respectively .

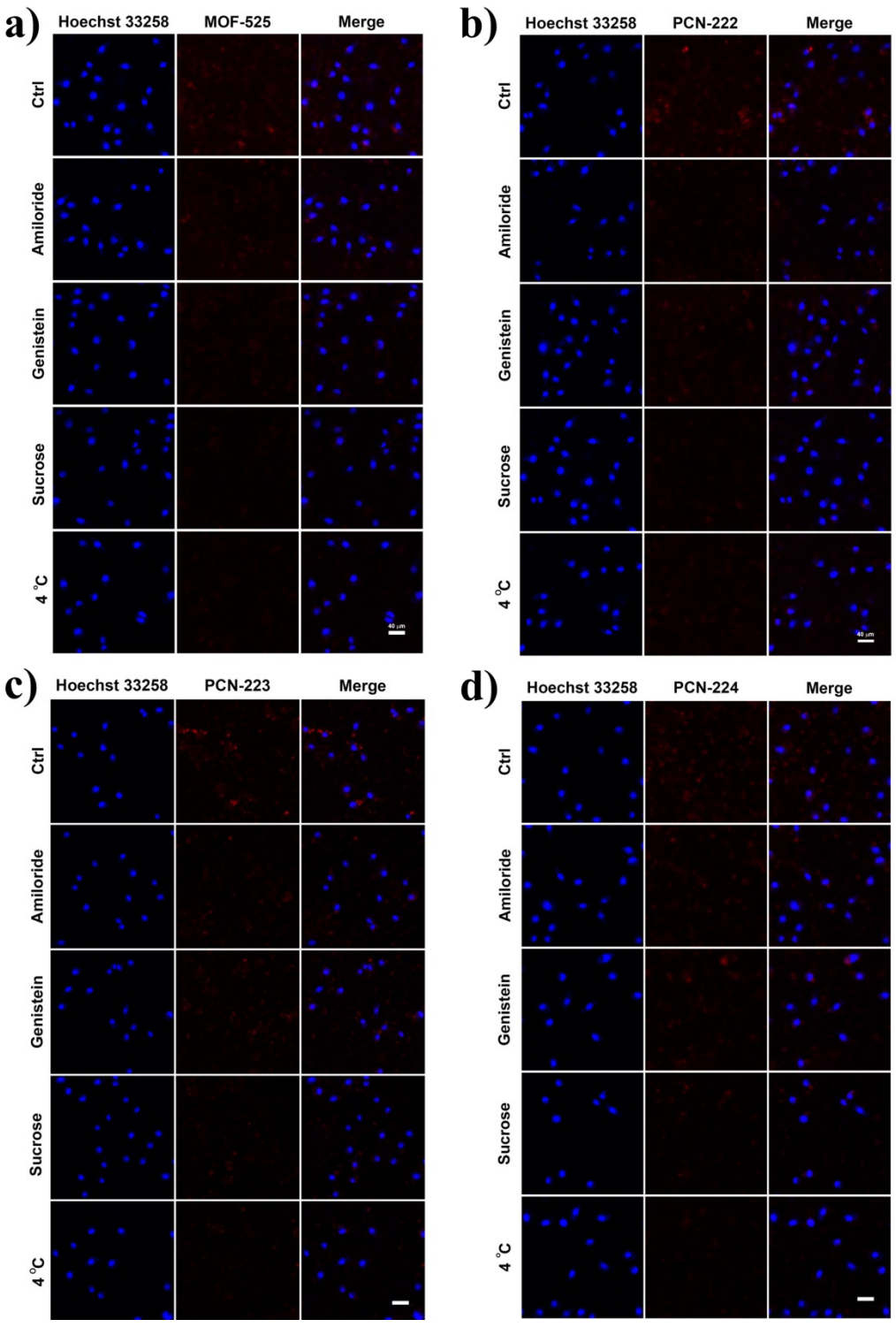

Figure S15. CLSM images of four TCPP-MOF isomers incubated with MCF-7 cells by adding different inhibitors at the same TCPP concentration of 40 μM TCPP for 2 h. Sucrose (SUC) for clathrin-mediated endocytosis, genistein (GEN) for caveolin mediated endocytosi, amiloride (AMI) for macropinocytosis, and 4 °C for energy-mediated endocytosis, respectively. Bar: 40 μm.

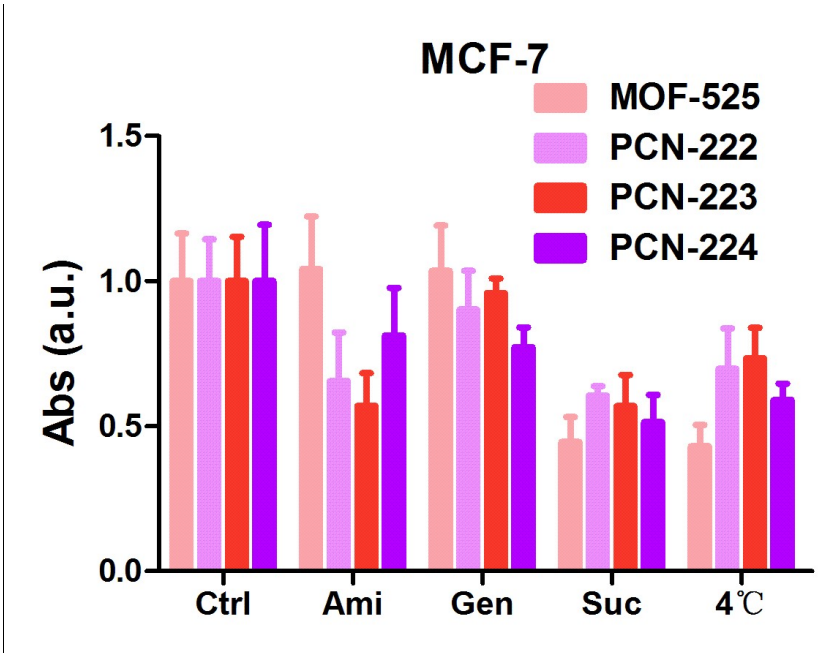

Figure S16. The UV quantification of four TCPP-MOF isomers incubated with MCF-7 cells by adding different inhibitors at the same TCPP concentration of 40 μM for 2 h.

Colocalization measured by CLSM

For lysosome colocalizaton visualization, before the cells were subjected to Hoechst 33258, pretreated with Lyso-Tracker Red for 1 h at 37 °C to stain lysosomes. Before the HeLa cells were observed via confocal laser fluorescence microscopy, the cells were rinsed three times with phosphate buffered saline solution (PBS) to remove excess MOFs samples.

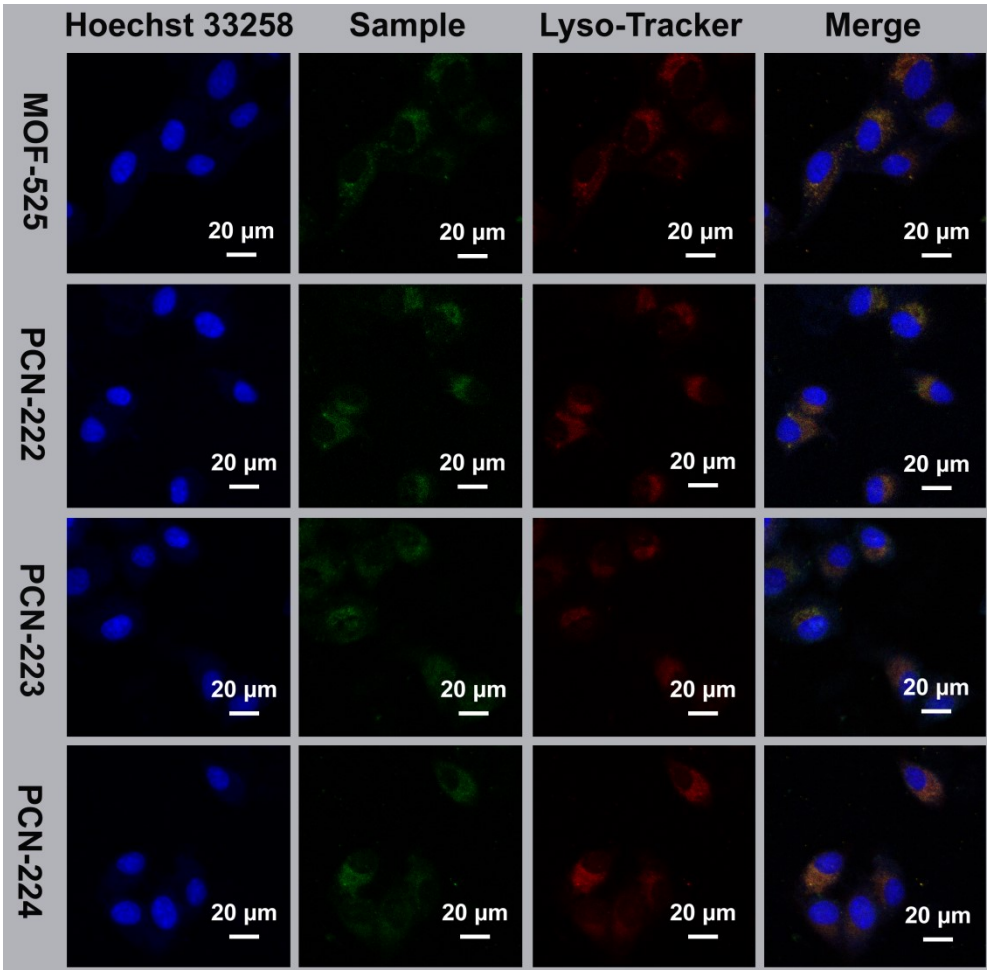

Figure S17. Lysosome colocalizaton of HeLa cells incubated with four TCPP-MOFs samples at the same TCPP concentration of 40 μM for 2 h at 37 °C.

The cytotoxicity test

MTT. The HeLa cells and MCF-7 cells were implanted in a 96-well plate with 100 μL of DMEM at a density of 2×10^4 cells per well for 12 h. Then, each TCPP-MOF samples with various concentration were added into each well of the plate in three groups and 100 μL of fresh DMEM was also added. After 2 h incubation, cells were illuminated by 635 nm laser lamp (power density of 0.47 W cm^{-2}) for 5 min. After 24 h intervals, 20 μL of the MTT solution (5 mg mL^{-1}) in PBS was added and the plate was incubated for another 4 h at 37 °C. After that, the supernatant and TCPP-MOF samples were removed, and 150 μL of dimethyl sulfoxide was added to each well to dissolve MTT formazan crystals. The absorbance of the formazan product was measured at 570 nm by a microplate reader (BioTek, EXL808).

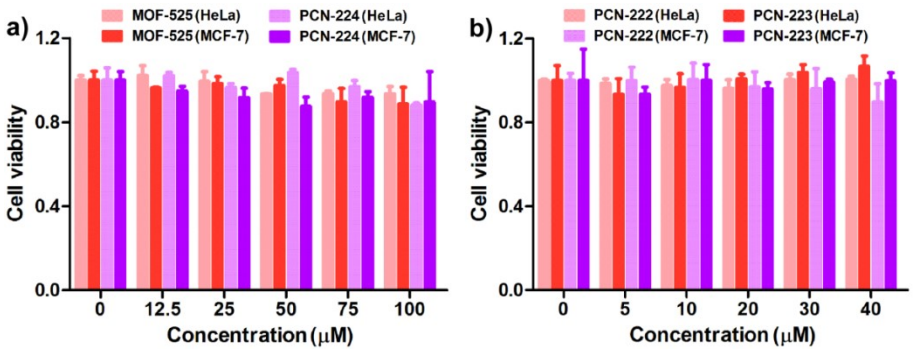

Figure S18. MTT results of the group of MOF-525 and PCN-224 and the group of PCN-222 and PCN-223 at the various TCPP concentration.

Table S4. The calculated photodynamic half inhibitory concentration (PC_{50}) (μM TCPP) of TCPP-MOF isomer against HeLa and MCF-7 cell lines.

	MOF-525	**PCN-222**	**PCN-223**	**PCN-224**
HeLa	27.8±2.0	10.9±0.7	18.8±3.3	40.4±3.1
MCF-7	43.4±3.8	7.4±0.3	12.5±0.3	52.8±13.2

Intracellular singlet-oxygen generation detection

Singlet-oxygen generation was detected by a cell-permeable ROS-sensitive fluorescent probe, 2′,7′-Dichlorodi-hydrofluorescein diacetate (DCFH-DA).[S11] DCFH-DA is non-fluorescent, but it could be rapidly oxidized to a fluorescent molecule (dichlorofluorescein, DCF) by singlet-oxygen. HeLa cells were incubated with TCPP-MOF samples (20 μM TCPP) for 2 h, and DCFH-DA (10 μM) was added and incubated for another 20 min. Then illuminated by 635 nm laser (power density of 0.47 W cm^{-2}) for 3 min. HeLa cells without illumination treatment were used as negative control. After the irradiation, the medium was replaced with culture medium. After removing the DCFH-DA-containing medium and washing three times, Cells was subjected to observation fluorescence by a NikonC1si laser scanning confocal microscopy.

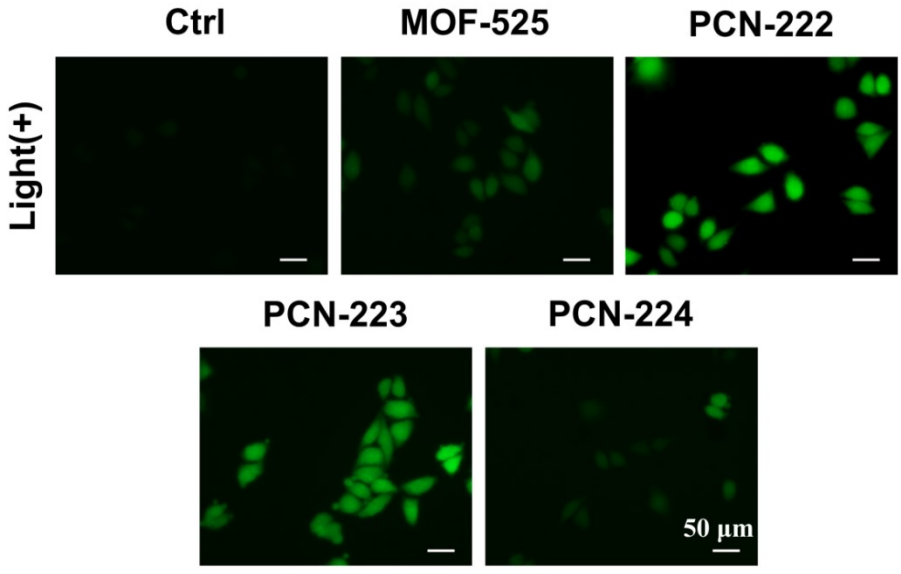

Figure S19. Intracellular singlet-oxygen generation detection of TCPP-MOF isomer by using the DCFH-DA detector. Scale bars: 50 μm.

Cell apoptosis and necrosis detection assays

The cell early and late apoptosis induced by PDT were quantified by FCM. Briefly, HeLa cells were cultured with TCPP-MOF samples (40 μM TCPP) for 2 h, and then illuminated by 635 nm laser (0.47 W cm^{-2}) for 5 min. The groups of PBS, TCPP-MOF samples without irradiation, and PBS with irradiation were set as negative control. After additional incubation for 24 h, cells were washed, harvested and collected, and stained with Annexin V-FITC and PI detection kit for about 0.5 h. Finally, the ratio analysis of apoptosis and necrosis were determined through flow cytometer.

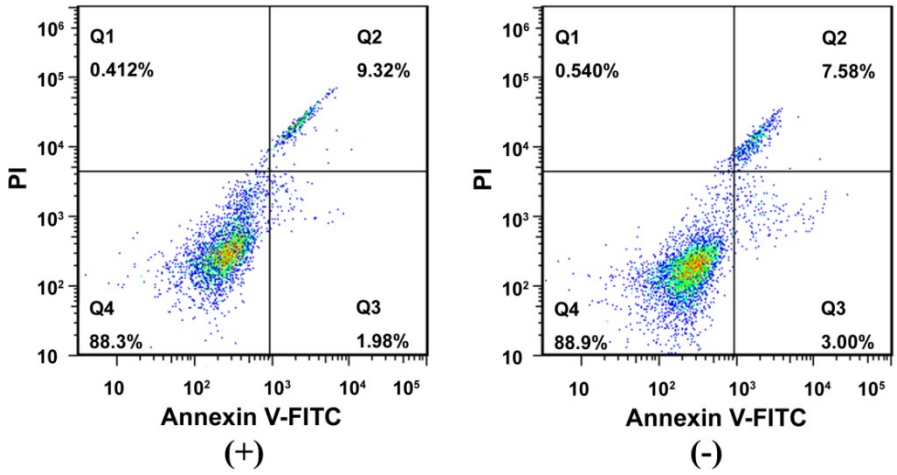

Figure S20. Flow cytometry analysis of HeLa cells incubated with blank with or without irradiation. The four areas represent the different phases of the cells: necrotic (Q1), late-stage apoptotic (Q2), early apoptotic (Q3), and live (Q4).

Calcein-AM/PI staining tests

To further demonstrate the PDT efficacy of as-synthesized TCPP-MOF samples, HeLa cells were stained with the calcein-AM/propidium iodide (PI) to identify live (green) and dead (red) cells. HeLa cells were incubated with TCPP-MOF samples (40 μM TCPP) for 2 h, and then illuminated by 635 nm laser (power density of 0.47 W cm^{-2}) for 5 min. TCPP-MOF samples without irradiation, PBS, and PBS with irradiation were set as negative control. After additional incubation for 24 h, the medium was removed and cells were washed gently. Then cells were incubated with Calcein-AM/PI for 30 min at room temperature, subsequently imaged by a NikonC1si laser scanning confocal microscopy.

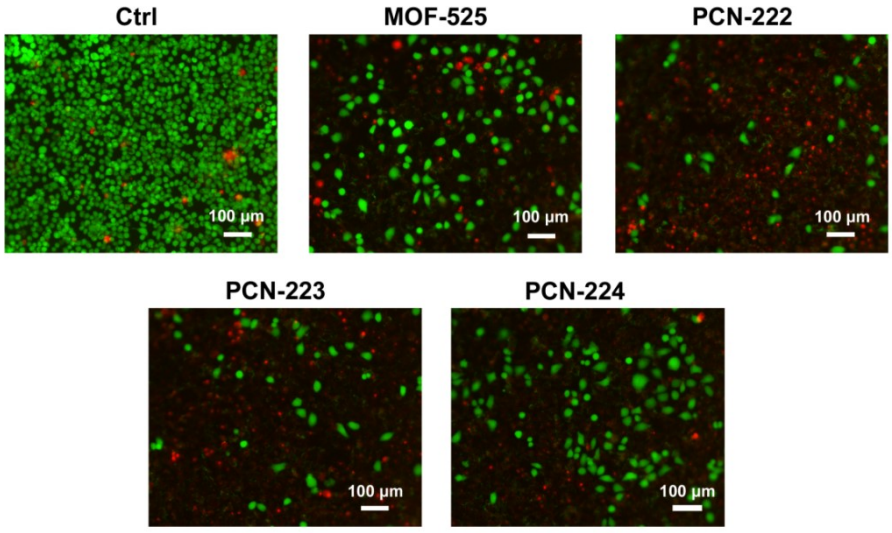

Figure S21. Fluorescence images of calcein-AM (green, live cells) and propidium iodide (red, dead cells) co-stained HeLa cells treated with control and TCPP-MOF isomers experimental groups with laser irradiation at 0.47 W cm^{-2} for 5 min, Scale bars: 100 μm.

Section S9. *In vivo* experiments

Animal Model. The healthy female Kunming mice (20–25 g) were purchased from the Laboratory Animal Center of Jilin University (Changchun, China) and maintained under required conditions. Animal care and handling procedures were carried out according to the guidelines of the Regional Ethics Committee for Animal Experiments.

Safety evaluation

The mice were randomly divided into five groups (n = 4): (1) PBS, (2) MOF-525, (3) PCN-222, (4) PCN-223, and (5) PCN-224. The mice were injected with PBS or TCPP-MOF samples (2 mg kg^{-1} TCPP) *via* the tail vein. Every two day, the body weights of mice were measured. The blood of mice was taken out for testing the level of alanine aminotransferase (ALT), serum aspartate transaminase (AST), uric acid (UA), urea (UREA) and creatinine (CREA). The blood of mice was also used for hematology analysis of WBC (10^9 L^{-1}), RBC (10^{12} L^{-1}), HGB (g L^{-1}), HCT (%), MCV (fL), MCH (pg), MCHC (g L^{-1}), PLT (10^9 L^{-1}).

Main organs (heart, liver, spleen, lung, and kidney) were collected, fixed in 4% paraformaldehyde solution, and then embedded in paraffin, sliced and stained with hematoxylin and eosin (H&E) to evaluate potential toxicity for the organs. Hemolytic rates of red blood cells after incubation with TCPP-MOF at various concentrations for 4 h at 37 ^oC. The samples were centrifuged at 12000 r/min for 30 min, and then the UV absorbance of the supernatant was measured at 570 nm by a microplate reader (BioTek, EXL808) (n=3).

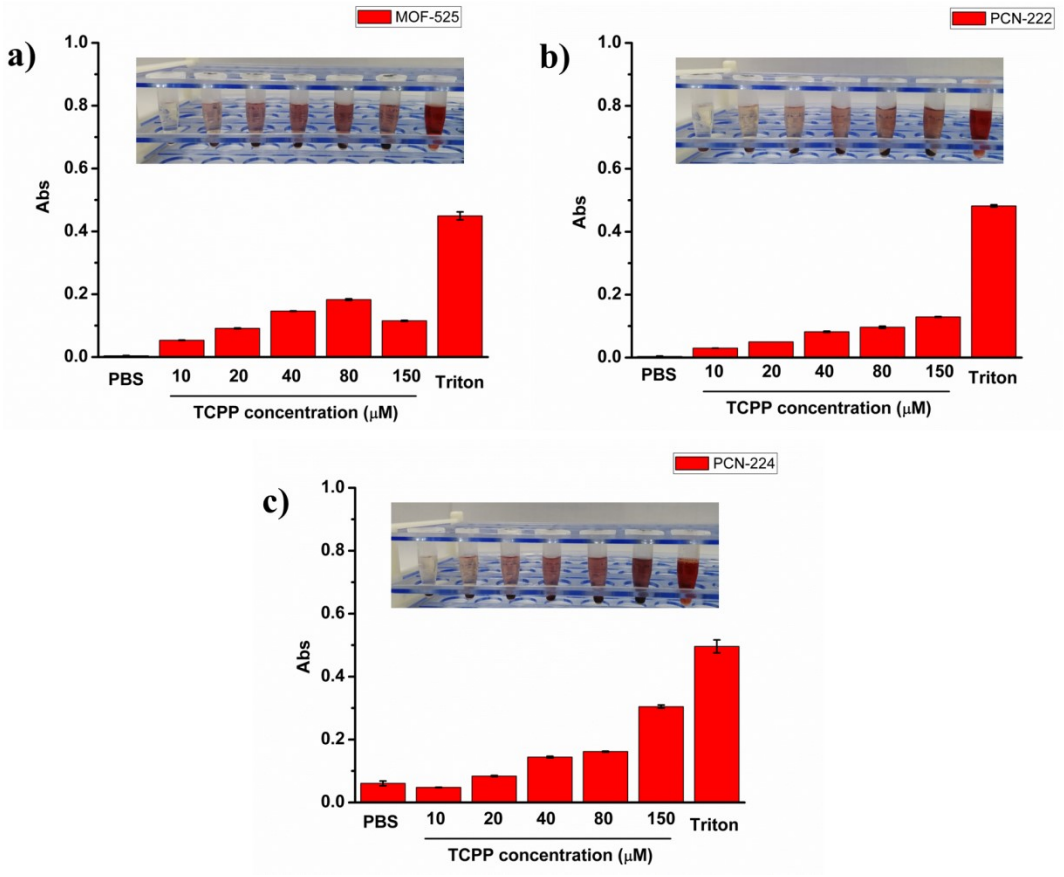

Figure S22. Hemolytic rates of red blood cells after incubation with TCPP-MOF at various concentrations for 4 h at 37 °C. (a) MOF-525. (b) PCN-222. (c) PCN-224.

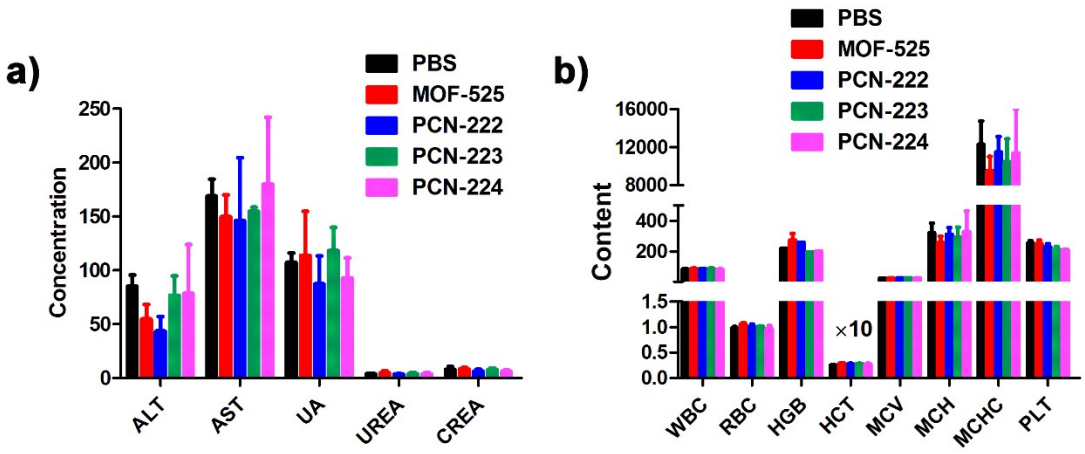

Figure S23. (a) Serum biochemistry analysis of alanine aminotransferase (ALT, U mL^{-1}), aspartate aminotransferase (AST, U mL^{-1}), creatinine (CREA, μmol L^{-1}) and uric acid (UA, μmol L^{-1}). (b) Hematology analysis results of WBC (10^9 L^{-1}), RBC (10^{12} L^{-1}), HGB (g L^{-1}), HCT (%), MCV (fL), MCH (pg), MCHC (g L^{-1}), PLT (10^9 L^{-1}).

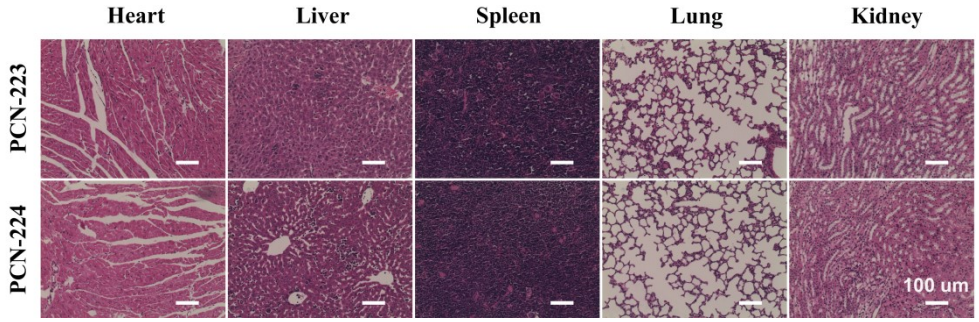

Figure S24. H&E staining images of major organ slices obtained from mice of PCN-223 and PCN-224. Scale bars: 100 μm.

Pharmacokinetics and Biodistribution

Tumor-free mice were randomly divided into four groups: (1) MOF-525, (2) PCN-222, (3) PCN-223, and (4) PCN-224. The mice were injected with TCPP-MOF samples (2 mg kg^{-1} TCPP) *via* the tail vein. Then, blood samples were taken at each predetermined time points and lysed with concentrated HNO_3 before the inductively coupled plasma mass spectrometry (ICP-MS) analysis. The major organs and tissue samples were excised at each selected interval. Subsequently, the collected samples were weighted and digested with concentrated HNO_3 at 140 °C for 24 h, and the content of Zr ions was quantified by ICP-MS. All the experiments were done in quadruplicate.

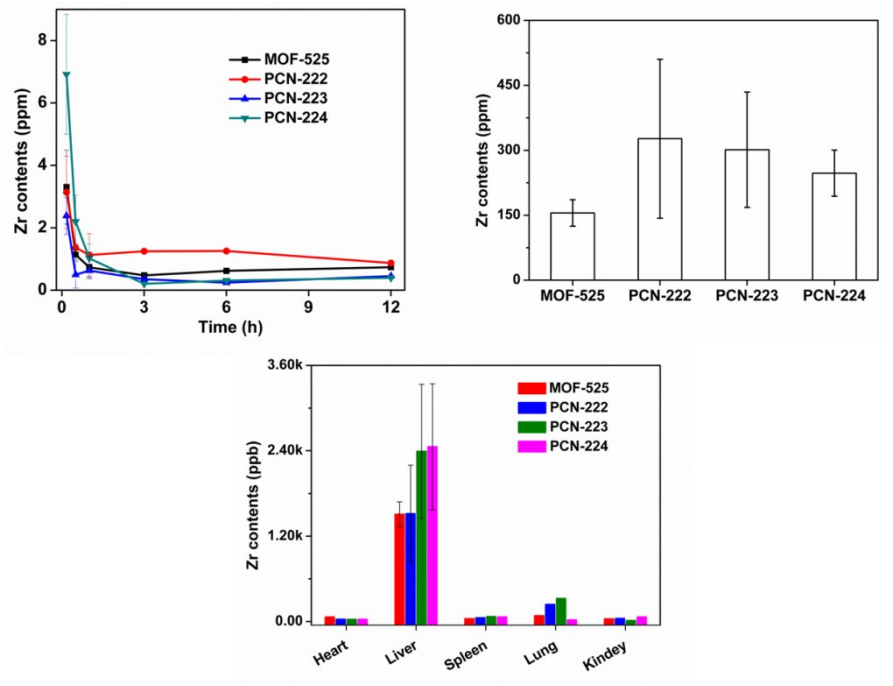

Figure S25. In vivo blood circulation and biodistribution of TCPP-MOF at different time points after intravenous injection by measuring the Zr contents through ICP-MS method.

Reference

S1. X. Zheng, L. Wang, M. Liu, P. Lei, F. Liu and Z. Xie, Nanoscale Mixed-Component Metal-Organic Frameworks with Photosensitizer Spatial-Arrangement-Dependent Photochemistry for Multimodal-Imaging-Guided Photothermal Therapy, *Chem. Mater.*, **2018**, 30, 6867-6876.

S2. X. Zheng, L. Wang, Y. Guan, Q. Pei, J. Jiang, Z. Xie, Integration of metal-organic framework with a photoactive porous-organic polymer for interface enhanced phototherapy, *Biomaterials,* **2020**, 235, 119792.

S3. W. Morris, B. Volosskiy, S. Demir, F. Gándara, P. L. McGrier, H. Furukawa, D. Cascio, J. F. Stoddart, and O. M. Yaghi, Synthesis, Structure, and Metalation of Two New Highly Porous Zirconium Metal-Organic Frameworks, *Inorg. Chem.* **2012**, 51, 6443-6445.

S4. D. Feng, Z. Gu, J. Li, H. Jiang, Z.Wei, and H. Zhou, Zirconium-Metalloporphyrin PCN-222: Mesoporous Metal-Organic Frameworks with Ultrahigh Stability as Biomimetic Catalysts, *Angew. Chem. Int. Ed.* **2012**, 51, 10307-10310.

S5. D. Feng, Z. Gu, Y. Chen, J. Park, Z. Wei, Y. Sun, M. Bosch, S. Yuan, and H. Zhou, A Highly Stable Porphyrinic Zirconium Metal-Organic Framework with shp-a Topology, *J. Am. Chem. Soc.* **2014**, 136, 17714-17717.

S6. D. Feng, W. Chung, Z. Wei, Z. Gu, H. Jiang, Y. Chen, D. J. Darensbourg, and H. Zhou, Construction of Ultrastable Porphyrin Zr Metal-Organic Frameworks through Linker Elimination*, J. Am. Chem. Soc.* **2013**, 135, 17105-17110.

S7. P. Deria, J. Yu, R. P. Balaraman, J. Mashni and S. N. White, Topology-dependent emissive properties of zirconium-based porphyrin MOFs, *Chem. Commun.,* **2016**, 52, 13031-13034.

S8. P. Deria, J. Yu, T. Smith, and R. P. Balaraman, Ground-State versus Excited-State Interchromophoric Interaction: Topology Dependent Excimer Contribution in Metal-Organic Framework Photophysics, *J. Am. Chem. Soc.* **2017**, 139, 5973-5983.

S9. Q. Guan, D. Fu, Y. Li, X. Kong, Z. Wei, W. Li, S. Zhang, and Y. Dong, BODIPY-Decorated Nanoscale Covalent Organic Frameworks for Photodynamic Therapy, *iScience* **2019**, 14, 180-198.

S10. D. Monti, D. Guarnieri, G. Napolitano, R. Piccoli, P. Nettic, S. Fusco, A. Arciello, Biocompatibility, Cells uptake and endocytosis pathways of polystyrenenanoparticles in primary human renal epithelial cells, *Journal of Biotechnology*, **2015**, 193, 3-10.

S11. X. Zheng, L. Wang, Q. Pei, S. He, S. Liu and Z. Xie, Metal-Organic Framework@Porous Organic Polymer Nanocomposite for Photodynamic Therapy, *Chem. Mater.*, **2017**, 29, 2374-2381.